Available online at www.sciencedirect.com
SCIENCE DIRECT®
ELSEVIER
Nuclear Instruments and Methods in Physics Research B 237 (2005) 301–306
NIM B Beam Interactions with Materials & Atoms
www.elsevier.com/locate/nimb

Damage effect of fluorine implantation on PECVD α-SiOC barrier dielectric

F.M. Yang [a], T.C. Chang [d,e,*], P.T. Liu [b,c], C.W. Chen [a], Y.H. Tai [b], J.C. Lou [a]

[a] *Institute of Electronics, National Chiao Tung University, Hsin-Chu, Taiwan, ROC*
[b] *Department of Photonics and Display Institute, National Chiao Tung University, Hsin-Chu, Taiwan, ROC*
[c] *National Nano Device Laboratory, 1001-1 Ta-Hsueh Rd., Hsin-Chu 300, Taiwan, ROC*
[d] *Department of Physics and Institute of Electro-Optical Engineering, National Sun Yat-Sen University, 70 Lien-hai Rd., Kaohsiung 804, Taiwan, ROC*
[e] *Center for Nanoscience and Nanotechnology, National Sun Yat-Sen University, Kaohsiung, Taiwan, ROC*

Available online 14 July 2005

Abstract

In this work the dielectric properties of plasma enhanced chemical vapor deposited (PECVD) amorphous SiOC (α-SiOC) films with various concentrations of oxygen are investigated for the barrier dielectric application. Experimental results show after fluorine (F) ion implanted into α-SiOC film, the leakage current in carbide film is increased due to the generation of trap centers. Afterwards, the traps can be effectively repaired after thermal annealing, leading to the decrease of leakage current further. From the extraction of the current–voltage (*J–E*) characteristics, the conducting mechanism of the leakage current obeys the Poole–Frenkel type behavior for intrinsic, F-implanted and thermally annealed samples. Also, the barrier height of the F-implanted and thermally annealed samples are extracted and exhibits a higher value than that of the intrinsic sample.
© 2005 Elsevier B.V. All rights reserved.

Keywords: PECVD; SiOC; Barrier dielectric; Poole–Frenkel; Implantation

1. Introduction

Copper (Cu) is a serious contamination source for both silicon and silicon oxide in interconnect applications [1,2]. To prevent Cu from diffusion into inter-metal dielectrics (IMD), Cu must be sealed using diffusion barriers [3,4]. A dielectric diffusion barrier layer is deposited on Cu and

* Corresponding author. Address: Department of Physics and Institute of Electro-Optical Engineering, National Sun Yat-Sen University, 70 Lien-hai Rd., Kaohsiung 804, Taiwan, ROC. Tel.: +886 7 5252000x3708; fax: +886 7 5253709.
E-mail address: tcchang@mail.phys.nsysu.edu.tw (T.C. Chang).

0168-583X/$ - see front matter © 2005 Elsevier B.V. All rights reserved.
doi:10.1016/j.nimb.2005.05.013

serves as the etch stop layer during the etching of trench or via of the next metal layer. Conventionally, silicon nitride (SiN_x) has been the barrier dielectric because of its barrier capability against ionic impurities, moisture resistance and chemical inertness. SiN_x has also been utilized as an etching stop layer and a final capping/passivation layer. However, SiN_x has a high dielectric constant (~8.0). To reduce the effective dielectric constant in the damascene structure, the amorphous oxygen-doped silicon carbide (α-SiOC), deposited by plasma enhanced chemical vapor deposition using tri-methyl-silane ($(CH_3)_3SiH$), has been investigated as the copper diffusion/drift barrier layer, hard mask and etching stop layer [5,6]. Also, amorphous oxygen-doped silicon carbide (α-SiOC) has lower dielectric constant (about 4–6) than that of silicon nitride. In this study, α-SiOC films were investigated to be utilized as the barrier dielectric. It is observed from the electrical characterization that oxygen-doped silicon carbide as a barrier dielectric prevents copper penetration after F ion implantation. Moreover, the influence of thermal treatments on electrical characterization of oxygen-doped silicon carbide was demonstrated in this work.

2. Experimental methods

The oxygen-doped silicon carbide films were deposited using tri-methyl-silane (3MS) in a PECVD system. The various concentrations of oxygen of the SiOC films were controlled by O_2 gas flow rate during PECVD deposition process. The flow rates of O_2 gas for samples SiOC-D1, SiOC-D2 and SiOC-D3 were 10%, 25% and 40%, respectively. During deposition, the pressure was controlled at 1.5 Torr with the temperature of 350 °C. The material analyses of oxygen-doped silicon carbide films were characterized by AES, FTIR and n&k analyzer. The refractive index is also measured by n&k analyzer. The electrical measurements were performed on the metal–insulator–semiconductor (MIS) structure with Al or Cu gate electrode. The permittivity of the dielectrics is determined by C–V 4284A precision LCR meter at 1 MHz frequency. The current–voltage (*I*–*V*) characteristics were measured using 4156C parameter analyzer. The Cu gate MIS capacitors were performed with the bias-temperature–stress (BTS) at 150 °C for 1000 s with gate electric field 4 MV/cm and 5 MV/cm to simulate and stimulate the diffusion of Cu ions. F ion implantation followed by 400 °C thermal annealing was explored to enhance the ability of preventing the penetration of Cu ions through α-SiOC films [7].

3. Results and discussion

The Auger electron spectrum (AES) was employed to detect the concentration of Si, C and O elements of SiOC films. In Fig. 1, the AES spectra of sample SiCO-D1 show that SiCO-D1 has the least oxygen concentration. The infrared spectrometry, performed from 400 to 4000 cm^{-1} by using Fourier transform infrared (FTIR) spectrometer, is calibrated to an unprocessed bare wafer, which is shown in Fig. 2 for determining the chemical structure of the silicon carbide films [8]. Si–C (780 cm^{-1}), Si–O (1000 cm^{-1}), $Si–CH_3$ (1250 cm^{-1}) and Si–H (2100 cm^{-1}) bonds are clearly exhibited in Fig. 2. The basic parameters for intrinsic samples and F-implanted samples with annealing are listed in Tables 1 and 2, respectively, where *n* represents the refractive index, *k* relative dielectric constant and *d* is the thickness of the films. The dielectric constant due to the electronic contribution is declined drastically with an

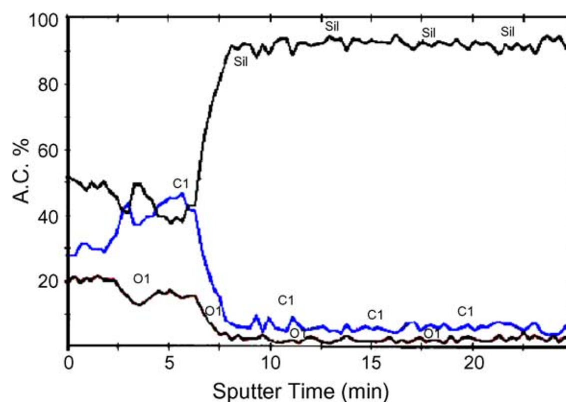

Fig. 1. Auger electron spectra of SiOC-D1.

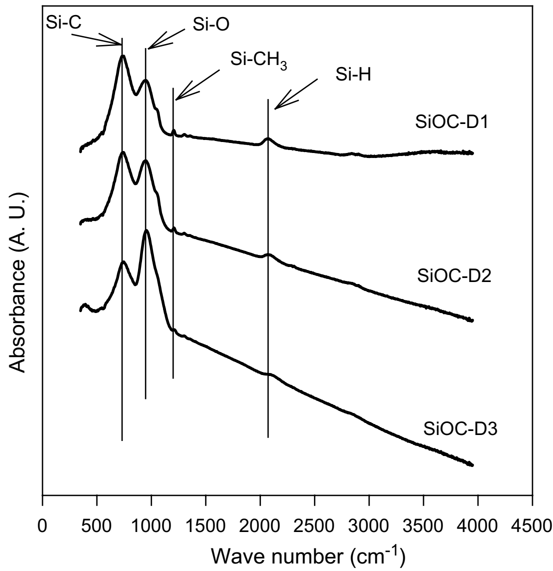

Fig. 2. FTIR of all samples (intrinsic) at RT.

Table 1
Basic parameters for intrinsic samples

	SiC	SiCO-D1	SiCO-D2	SiCO-D3
k	4.54	4.51	4.02	3.14
n	1.88	1.737	1.741	1.749
d (nm)	100	100.1	100.5	104.5

Table 2
Basic parameters for F-implanted with annealed samples

	SiCO-D1	SiCO-D2	SiCO-D3
k	5.31	4.77	2.91
n	1.744	1.852	2.068
d (nm)	105.6	103.2	93.3

increased O_2 flow rate. The reduction of the dielectric constant of the α-SiOC film caused by the electronic contribution is attributed to the replacement of Si–C by Si–O bonds. The higher electronegativity of oxygen atom decreases the polarizability of the bonds and results in a lower *k*-value [9]. As shown in Fig. 3, the leakage current of SiC is larger than that of the oxygen-doped SiC in high electric field. It exhibits SiCO-D3 has the largest leakage current and SiCO-D1 has the smallest leakage current. Current density–electric field (*J*–*E*) characteristic of SiOC-D1 for F-implanted and intrinsic samples at RT and 150 °C are shown in Fig. 4. It is found that the leakage current was increased after F ion implantation in SiCO-D1.

The comparison of *J*–*E* characteristics at 150 °C of D1, D2 and D3 after implantation is

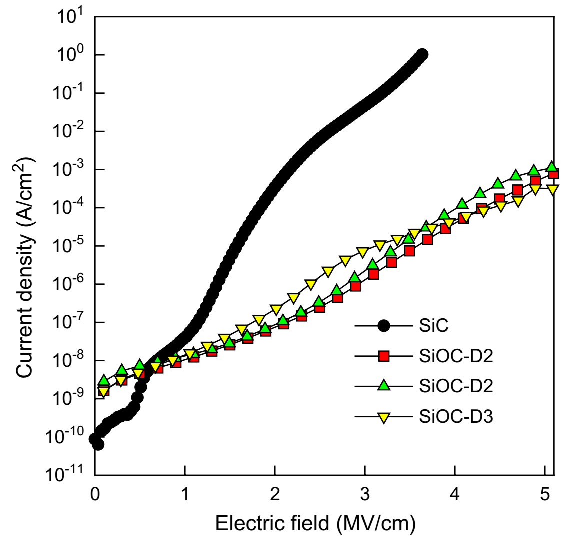

Fig. 3. Current density–electric field curves of the intrinsic samples.

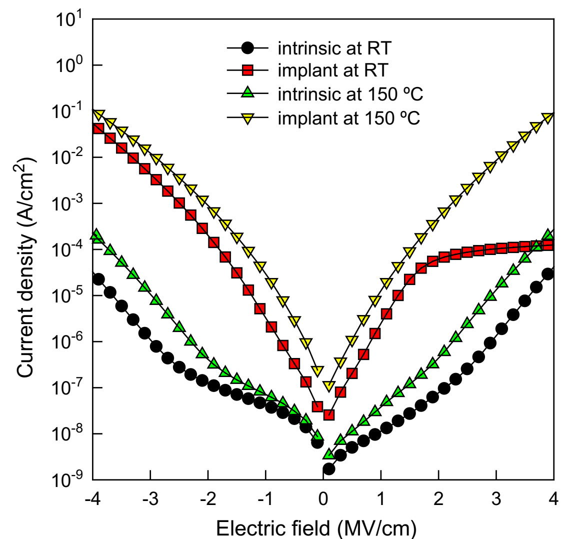

Fig. 4. Current density–electric field of SiOC-D1 for intrinsic and F ion implant at room temperature and 150 °C.

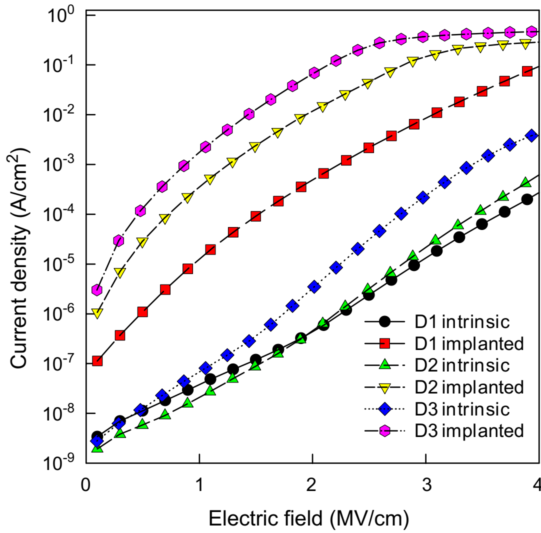

Fig. 5. Comparison of current density–electric field curves of D1, D2 and D3 after F implantation at 150 °C.

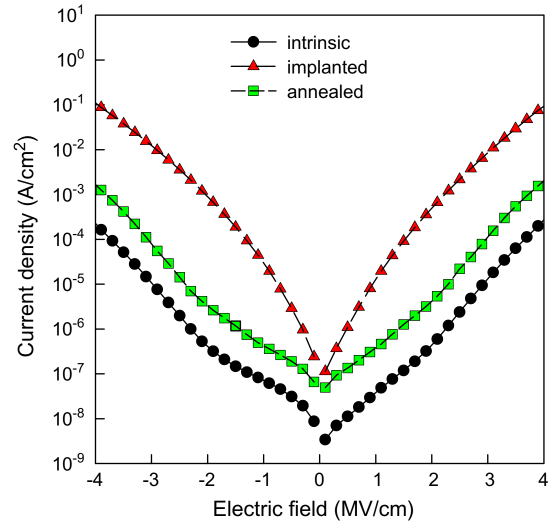

Fig. 6. Current density–electric field curves of D1 after thermal annealing at 400 for 3 h.

shown in Fig. 5. It is inferred that F ion implantation causes the increasing quantities of traps in silicon carbide films that raises the leakage current. SiCO-D1 after F ion implantation were transferred into a quartz furnace at 400 °C for 3 h in N_2 ambient [10]. After the thermal annealing, it is found that the leakage current is lower than that of the pre-annealed samples in Fig. 6. The traps were repaired which leads to the decrease of leakage current after thermal annealing. The electrical results of BTS measurements are shown in Fig. 7. It shows that the thermal annealing helps to lower the leakage current for the stress field of 4 MV/cm after F ion implantation but not for 5 MV/cm. Thermal annealing has the ability to mend traps caused from F ions. However, because SiCO-D3 contains more oxygen atoms than that of SiCO-D1 and SiCO-D2, oxygen atoms help F ions grab free electrons, which results in that the leakage current is not lowered even with thermal annealing after F ion implantation [11].

To investigate the leakage mechanisms of the conduction of SiOC films, there are two typical leakage current mechanisms such as Schottky–Richardson emission and Poole–Frenkel emission analyzed in the electrical results of the samples. The linear variations of the $\ln(J)$–$E^{1/2}$ or $\ln(J/E)$–

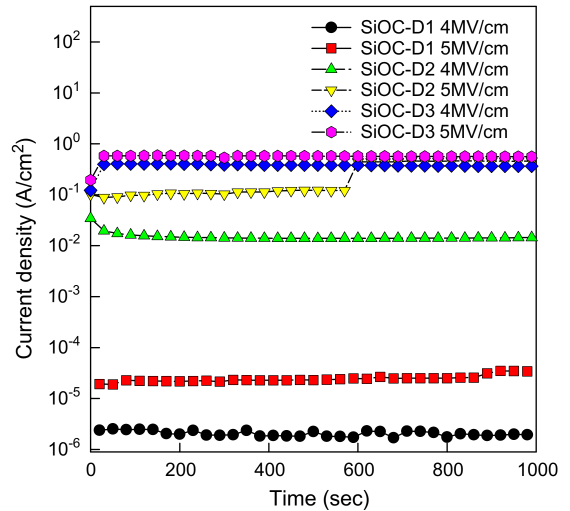

Fig. 7. Current density–electric field curves of F-implanted with annealing samples after BTS.

$E^{1/2}$ current correspond to either Schottky–Richardson emission or Poole–Frenkel emission. The Schottky–Richardson emission is defined by the thermionic effect caused by the electron transport across the potential energy barrier via field-assisted lowering at a metal–insulator interface. The current density (J) in the Schottky emission can be formulated by the following equation:

$$J = A^*T^2 \exp\left(\frac{\beta_s E^{1/2} - \phi_s}{k_B T}\right), \quad (1)$$

where $\beta_s = (e^3/4\pi\varepsilon_0\varepsilon_r)^{1/2}$, ε_0 the dielectric constant of free space ($\varepsilon_0 = 8.854 \times 10^{-14}$ F/cm), ε_r the high frequency relative dielectric constant, A^* the effective Richardson constant, T the absolute temperature, E the applied electric field, ϕ_s the contact potential barrier and k_B is the Boltzmann constant ($k_B = 1.38 \times 10^{-23}$ J/K). The Poole–Frenkel emission is due to field-enhanced thermal excitation of trapped electrons in the insulator into the conduction band. The current density (J) can be expressed by

$$J = J_0 \exp\left(\frac{\beta_{PF} E^{1/2} - \phi_{PF}}{k_B T}\right), \quad (2)$$

where $J_0 = \sigma_0 E$ is the low-field current density, σ_0 the low-field conductivity, $\beta_{PF} = (e^3/4\pi\varepsilon_0\varepsilon_r)^{1/2}$, and ψ_{PF} is the height of trap potential well. In theory, the value of β_{PF} is twice as large as the value of β_s. The statement is shown by the following two equations:

$$\beta_{PF} = \sqrt{\frac{e^3}{\pi\varepsilon_0\varepsilon_r}} \quad \text{(theoretical value)}, \quad (3)$$

$$\beta_s = \sqrt{\frac{e^3}{4\pi\varepsilon_0\varepsilon}} \quad \text{(theoretical value)}. \quad (4)$$

ε_r among Eqs. (3) and (4) can be obtained by C–V measurement with the equation

$$C = \varepsilon_r\varepsilon_0 \frac{A}{t} \quad (5)$$

The J–E curves are transformed to $\ln(J/E)$ versus $E^{1/2}$ for Poole–Frenkel emission and $\ln(J)$ versus $E^{1/2}$ for Schottky emission. The slope (β/k_BT) of the curve $\ln(J/E)$ versus $E^{1/2}$ and $\ln(J)$ versus $E^{1/2}$ was calculated. Distinction between the two leakage current mechanisms can be executed by comparing the theoretical value of β_{PF} or β_s with the experimental value of β. Fig. 8 shows $\ln(J/E)$–$E^{1/2}$ curves of SiCO-D1 (STD) at various temperatures to get β_{PF}. From Eq. (2), the current density is given as follows:

$$\ln\left(\frac{J}{E}\right) = \ln\sigma_0 + \left(\frac{\beta_{PF}E^{1/2} - \phi_{PF}}{k_B}\right)\frac{1}{T}. \quad (6)$$

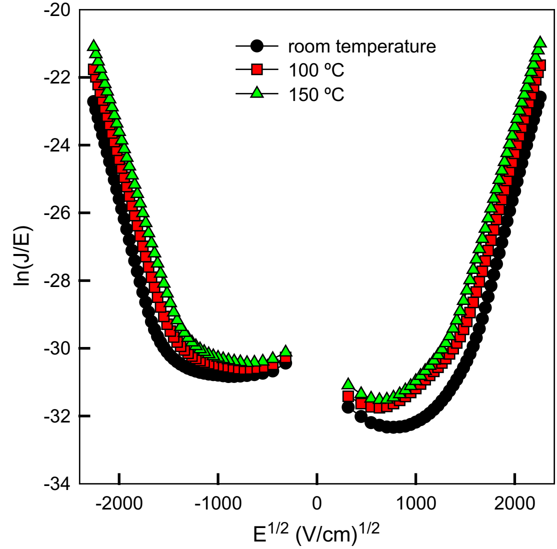

Fig. 8. $\ln(J/E)$–$E^{1/2}$ curves of SiCO-D1 (intrinsic) at various temperature.

Table 3
φ_{PF} and β_{PF} of SiCO-D1 intrinsic and F-implanted with annealing samples

	β_{PF} ($\times 10^{-23}$)	φ_{PF} (eV)
Intrinsic 4 MV/cm	5.73	0.3084
F-implanted with annealing 4 MV/cm	4.32	0.466

The relation of $\ln(J/E)$–$(1/T)$ can be obtained and via the slope of the straight line portion of the curve, the height of the energy barrier can be extracted as shown in

$$\phi_{PF} = \beta_{PF}\sqrt{E} - \text{slope} \times k_B \quad (7)$$

The experimental and theoretical β values are compared with each other. It is found the conduction mechanism of SiCO-D1 (STD) is Poole–Frenkel emission whether intrinsic or F-implanted with annealing samples. ϕ_{PF} values of the intrinsic SiCO-D1and F-implanted with annealing samples are shown in Table 3.

4. Conclusions

F ion implantation causes the increasing quantities of traps in silicon carbide films and raises the

leakage current after implantation. After thermal annealing, it is found that the leakage current is lower than that before thermal annealing. The traps are repaired which leads to the decrease of leakage current after thermal annealing. Thermal annealing has the ability to mend traps caused from F ions. From the fitting of the current–voltage characteristics, the conducting mechanism of the leakage current obeys Poole–Frenkel conduction for intrinsic or F-implanted and with annealing samples. It is found SiCO-D1 holds Poole–Frenkel conduction whether intrinsic or F-implanted with annealing samples. The barrier height of the F-implanted and annealed sample is extracted and raised to a higher value than that of the intrinsic sample.

Acknowledgements

This work was performed at National Nano Device Laboratory and the National Synchrotron Radiation Research Center and was supported by National Nano Device Laboratory under Contract No. 92A0500001 and the National Science Council of the Republic of China under Contract Nos. NSC93-2112-M-110-008.

References

[1] N. Kawakami, Y. Fukumoto, T. Kinoshita, K. Suzuki, K.-I. Inoue, in: Proceedings of the IEEE 2000 International Interconnect Technology Conference, 2000, p. 143.
[2] P.T. Liu, T.C. Chang, S.M. Sze, F.M. Pan, Y.J. Mei, W.F. Wu, M.S. Tsai, B.T. Dai, C.Y. Chang, F.Y. Shih, H.D. Huang, Thin Solid Films 332 (1998) 345.
[3] A. Cros, M.O. Aboelfotoh, K.N. Tu, J. Appl. Phys. 67 (1990) 3328.
[4] T. Furusawa, N. Sakuma, D. Ryuzaki, S. Kondo, K. Takeda, S.-T. Machida, K. Hinode, in: Proceedings of the IEEE 2000 International Interconnect Technology Conference, 2000, p. 222.
[5] M.T. Kim, J. Lee, Thin Solid Films 303 (1997) 173.
[6] V. Chu, N. Barradas, J.C. Soares, J.P. Conde, J. Jarego, P. Brogueira, J. Rodriguez, J. Appl. Phys. 78 (1995) 3164.
[7] P.T. Liu, T.C. Chang, Y.L. Yang, Y.F. Cheng, S.M. Sze, IEEE Trans. Electron. Dev. 47 (2000) 1733.
[8] R.A.C.M. van Swaaij, A.J.M. Berntsen, W.G.J.H.M. van Sark, H. Herremans, J. Bezemer, W.F. van der Weg, J. Appl. Phys. 76 (1994) 251.
[9] Y.W. Koh, K.P. Loh, L. Rong, A.T.S. Wee, L. Huang, J. Sudijono, J. Appl. Phys. 93 (2003) 1241.
[10] D.S. Kim, Y.H. Lee, Thin Solid Film 261 (1995) 192.
[11] B.K. Hwang, M.J. Loboda, G.A. Cerny, R.F. Schneider, J.A. Seifferly, T. Washer, in: Proceedings of the IEEE 2000 International Interconnect Technology Conference, 2000, p. 52.